

Deep Inverse Design for High-Level Synthesis

Ping Chang*, Tosiron Adegbiya*, Yuchao Liao*, Claudio Talarico[§], Ao Li*[†], Janet Roveda*^{†‡}

*Department of Electrical & Computer Engineering, The University of Arizona, Tucson, AZ, USA

[†]Bio5 Institute, The University of Arizona, Tucson, AZ, USA

[‡]Department of Biomedical Engineering, The University of Arizona, Tucson, AZ, USA

[§]School of Engineering & Applied Science, Gonzaga University, Spokane, WA, USA

Abstract—High-level synthesis (HLS) has significantly advanced the automation of digital circuits design, yet the need for expertise and time in pragma tuning remains challenging. Existing solutions for the design space exploration (DSE) adopt either heuristic methods, lacking essential information for further optimization potential, or predictive models, missing sufficient generalization due to the time-consuming nature of HLS and the exponential growth of the design space. To address these challenges, we propose *Deep Inverse Design for HLS (DID4HLS)*, a novel approach that integrates graph neural networks and generative models. DID4HLS iteratively optimizes hardware designs aimed at compute-intensive algorithms by learning conditional distributions of design features from post-HLS data. Compared to four state-of-the-art DSE baselines, our method achieved an average improvement of 42.5% on average distance to reference set (ADRS) compared to the best-performing baselines across six benchmarks, while demonstrating high robustness and efficiency.

Index terms: ADRS, deep learning, generative model, GNN, HLS, IR, Pareto front

Keywords: deep learning, GAT, HLS, inverse design, post-HLS IR, VAE

I. INTRODUCTION

The increasing complexity of circuit designs, compounded by stringent time-to-market imperatives, underscores the demand for advanced design automation [1]. High-level synthesis (HLS) is an increasingly popular and pivotal solution that facilitates the conversion of algorithms expressed in high-level languages (HLLs) such as C/C++/SystemC into hardware descriptions [2]. However, HLS as a multi-objective optimization problem (MOOP) necessitates expertise and experience to navigate the optimization among the conflicting objectives such as latency and area [3], [4]. Consequently, there is a high demand for the automation of the design space exploration (DSE) process to address the complex tuning challenges for pragmas (or directives).

Heuristic methods offer rapid implementations to yield improved designs [5]–[10]. However, their effectiveness is limited by the lack of a thorough understanding of the behaviors of HLS tools. We need to understand how operations are scheduled in order to estimate design performance, but the scheduling information is only available after the HLS process [11]. Recently, graph neural networks (GNNs) have been employed for code analysis to predict synthesis results, demonstrating advantages over the preceding DSE methods [12]–[16]. Compilers transform algorithms in HLL

into platform-independent intermediate representations (IRs) that encapsulate semantic information [17]–[19]. They are subsequently transformed into control and data flow graphs (CDFGs) for GNN training [20], [21]. However, three critical issues hinder the effectiveness of these methods:

1) The exponential increase in design space size and the time-consuming nature of HLS pose challenges in acquiring sufficient synthesis data for training high-generalization models [15], [22].

2) Current methods are tied to specific IR compilers. Using these methods in a different toolchain introduces representation discrepancies. For example, GNNs adopting LLVM IR [17] does not match HLS tools operating Hector [23]. Besides, even when the compilers match, changes in compiler versions require additional workload on the methods. These discrepancies lead to ineffective graph feature extraction [3].

3) The IRs do not adequately contain HLS information, which prevents them from effectively representing design variations [3]. As a result, the models leveraging IRs may not fully exploit the design space, leading to suboptimal designs.

Gradient-based inverse design has been widely adopted to retrieve the nanophotonic device designs with desired quality of results (QoR) from large design spaces [24], [25]. However, the inherent discrete nature of HLS design spaces keeps from applying the inverse design to DSE for HLS. Although several recent approaches approximated discrete spaces with continuous spaces [26], [27], they are not feasible for the inverse design in HLS due to the fact that the pragma effect on the QoR is non-monotonic [13].

To address these challenges, we propose a novel method called *Deep Inverse Design for HLS (DID4HLS)*. DID4HLS focuses on choosing the best pragma configurations of the compute-intensive algorithms to achieve designs that minimize the objectives of latency and area. We construct the design space with the pragmas of pipelining, loop unrolling, array partitioning, and function inlining. The uniqueness of DID4HLS lies in its strategy to work on a distribution that samples pragma configurations, with constraints that prevent redundant design samples according to the strategies of HLS tools, such as interactions between pipelining and loop unrolling. Initially, DID4HLS uses a Uniform pragma distribution to explore a wide range of design possibilities. It then iteratively synthesizes batches of designs generated from the updated pragma distributions, resulting in the IRs that are generally represented in CDFG and crucial in deriving their final hardware designs [28], [29]. In this work, we call these IRs as

post-HLS IRs (PIRs). These PIRs, along with data on their objectives, are collected into a dataset which is used to train the objective predictors based on Graph Attention Network v2 (GATv2) [30]. Furthermore, *DID4HLS* adopts Variational Autoencoder (VAE) to learn the distribution of design features that determine design performance. They are extracted from the PIRs by the GATv2 models. This training is conditioned on the pragma distributions. Through this process, *DID4HLS* effectively converges the pragma distribution to approximate Pareto front [3].

In summary, our work addresses the three aforementioned limitations of the prior works as follows:

- 1) By realizing inverse design, *DID4HLS* requires only a limited synthesis budget to achieve well-optimized designs, thereby significantly speeding up the synthesis process.
- 2) Compared to the methods with code analysis, *DID4HLS* operates PIRs and avoids representation discrepancies due to reliance on the IR compilers different from the ones adopted by the targeted HLS platforms.
- 3) In contrast to IRs, PIRs encapsulate essential hardware descriptions and scheduling information, reflecting design variations, leading to an effective DSE process.

We evaluated *DID4HLS* through rigorous experiments and quantified its performance in comparison to several prior works. Our results revealed significant improvements in the quality of the Pareto fronts generated by *DID4HLS*. In comparison to the best-performing DSE baselines, *DID4HLS* improves the average distance to the reference set (ADRS) by 42.5% on average over the baselines for six benchmarks adapted from Polybench [31] and MachSuite [32]. That is, *DID4HLS* significantly outperforms the state-of-the-art in achieving a close Pareto front to the optimal. The comparative experiments also demonstrate the high robustness and efficiency of our method. Furthermore, to validate the construction of *DID4HLS*, we also conducted an ablation study to explore the benefits of using PIRs and VAE. Results show that our approach achieved an average improvement of 48.0% over the best-performing ablation configurations.

II. BACKGROUND

A. Post-HLS Intermediate Representation

The initial HLS phase parses algorithms in HLL into virtual instruction sets called intermediate representations. Subsequent phases entail specifying the order and timing of these instructions under predefined constraints to generate PIRs [28], [29]. PIR is a comprehensive representation of the synthesized design in the CDFG format and accurately describes the hardware designs. Consequently, we use PIR to capture hardware design variations induced by pragmas. PIR CDFG is composed of nodes and edges, each labeled with specific types and attributes. A toylike code is illustrated in Fig. 1 (a) with no pragma applied, and its corresponding PIR generated through Vitis HLS [33] is illustrated in Fig. 1 (b). Node attributes include node types, bitwidths, and consts, while edge attributes include edge types and data flow directions. For example, the node *add_In7* of type 0, indexed at 18, denotes an *add* operation with a bitwidth of 3. The edge indexed at 40 is of type 2.

```
void foo(int in_1[4], int in_2[4], int out[4]){
    for(int i=0; i<4; i++){
        out[i]=in_1[i]+in_2[i];
    }
}
```

(a)

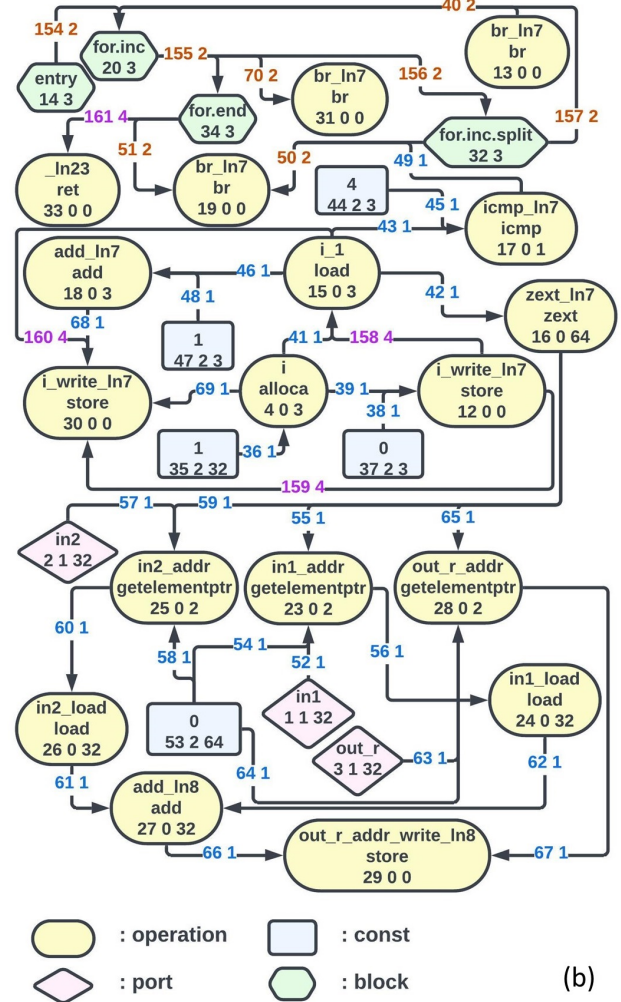


Fig. 1. (a) A toylike code example. (b) PIR of the code.

B. Graph Attention Networks

With the aid of the attention mechanism [34], Graph Attention Networks (GATs) update node features by learning weighted interactions among nodes and edges [35]:

$$e(\mathbf{h}_i, \mathbf{h}_j) = \text{LeakyReLU}(\mathbf{a}^\top [\mathbf{W}\mathbf{h}_i \parallel \mathbf{W}\mathbf{h}_j]) \quad (1)$$

where \mathbf{a} and \mathbf{W} are trainable parameters, \mathbf{h} denotes node features, i denotes the query node index, j denotes the key node index, and \parallel represents concatenation. Bold font represents matrix or vector in this work. Subsequently, aggregation of all node features gives graph features that are crucial for graph-based DSE methods [13]. However, Brody et al. highlighted a significant drawback in GAT, termed static attention [30], wherein attention rankings of queries collapse toward the dominant key node. This phenomenon arises due to the calculation of attention weights by a single-layer perceptron, as outlined in Eq. 1, where both linear transformation and activation maintain monotonicity, keeping the rankings of the keys. Despite

the introduction of multi-heads in GAT to introduce limited variation in attention rankings, the attention mechanism still experiences a loss of expressiveness. To address this issue, GATv2 proposes the substitution of the operation \mathbf{a} as follows [30]:

$$e(\mathbf{h}_i, \mathbf{h}_j) = \mathbf{a}^\top \text{LeakyReLU}([\mathbf{W}\mathbf{h}_i \parallel \mathbf{W}\mathbf{h}_j]) \quad (2)$$

thereby transforming the single-layer perceptron into an MLP. This modification allows for the approximation of a function capable of selecting any mappings among nodes [36], resulting in dynamic attention. Consequently, we employ GATv2 to extract graph features in our work.

C. Variational Autoencoder

Variational Autoencoder (VAE) is an encoder-decoder methodology [37] for variational inference [38], aimed at generating data within the distribution of input data \mathbf{x} . The encoder models the posterior $q(\mathbf{z}|\mathbf{x})$. The decoder models the likelihood $p(\mathbf{x}|\mathbf{z})$ and maps prior samples into the data within the targeting distribution. Its training objective is expressed below:

$$\begin{aligned} \operatorname{argmin}_{\mu, m, v} \{ & E_{q(\mathbf{z}|\mathbf{x})} \left[\frac{\|\mathbf{x} - \mu(\mathbf{z})\|_2^2}{2c} \right] \\ & - \sum_i \frac{1}{2} [1 + \log v_i(\mathbf{x}) - v_i(\mathbf{x}) - m_i^2(\mathbf{x})] \} \end{aligned} \quad (3)$$

where the function μ maps prior sample into the mean of $p(\mathbf{x}|\mathbf{z})$ at the bottleneck. Hyperparameter c governs the variance of $p(\mathbf{x}|\mathbf{z})$, while the functions m_i and v_i calculate the mean and variance, respectively, of the i -th dimension of $\mathbf{z} \sim q(\mathbf{z}|\mathbf{x})$. By combining conditioning variables into latent samples, VAE learns conditional distributions.

III. PROBLEM DEFINITION

Because HLS optimization is a MOOP, a single distribution is unable to cover the whole Pareto front. For instance, in the context of the trade-off between latency and area, the distribution prioritizing low latency might be significantly different from the one prioritizing low area. In order to approximate Pareto front, we pre-define a set of optimization weights λ sweeping from 0 to 1 and we denote the k -th weight as λ_k .

We aim to find a design d with the minimal cost for each weight defined as:

$$\mathbf{c}_k = \lambda_k l + (1 - \lambda_k) a \quad (4)$$

where l and a denote the standardized latency and area of d . The mean and standard deviation of latency and area for their standardization are obtained from the designs that are high-level synthesized during the experiments.

We create a vector set Θ in which the vector Θ_k corresponds to λ_k , as a pragma distribution from which pragma configurations are sampled. Each configuration combines with the algorithm in HLL into a design d from a pre-defined design space S . Our goal is to identify Θ_k that yields designs close to the optimal design:

$$\mathbf{d}_k^* = \min_{\mathbf{c}_k} d \in S \quad (5)$$

Considering the vast size of S and the time-consuming nature of HLS, we adopt an iterative process in which d is sampled with a lower cost mean $E[\mathbf{c}_k | \Theta_k]$ to approach \mathbf{d}_k^* . Therefore, we need to realize an algorithm A that updates Θ_k in iterations:

$$\begin{aligned} E[\mathbf{c}_k | \Theta_k^{i+1}] &< E[\mathbf{c}_k | \Theta_k^i] \\ \Theta_k^{i+1} &= A(\cup_j \{[l, a, \Theta_k]_d\}_j) \\ i &\in \mathbb{N} \\ j &= 1, 2, \dots, i \end{aligned} \quad (6)$$

IV. METHODOLOGY

A. Design Space Interface

To start the optimization process targeting pipelining, loop unrolling, array partitioning, and function inlining, an interface is established between algorithms in C++ and our method. Loops within the C++ code files are labeled. The arrays, denoted by `arr`, introduced below are user-defined that determine the design space S . `arrnest` describes how the loops nest. An example code with loop labels for HLS is shown in Fig. 2. `arrnest = [-1, 0, 1]` means the structure of the three loops. Here, `arrnest[2] = 1`, `arrnest[1] = 0`, and `arrnest[0] = -1` mean that the loop of index 2 is nested under the loop of index 1, and both are nested under the loop of index 0. `arrunroll` contains user-defined loop unrolling factors. For example, `arrunroll = [[1, 2], [1, 2, 4], [1, 2, 4, 8]]` means that `arrunroll[0] = [1, 2]` allows the loop of index 0 to be unrolled with a factor of 1 or 2, and the other two subarrays are for the rest loops in order. `arrpipeline` contains probabilities for each loop to be pipelined. `arrii` contains initiation intervals for a loop if it is pipelined. `arrinterface` specifies the arrays, at the interface of the top functions, to be partitioned with the type of block or cyclic. `arrp_itf` contains their array partitioning factors. `arrinline` contains probabilities for each function to be inlined. S determines the initialization of Θ which is then mapped to align with the deep models, rendering the method inherently self-adaptive. To maximize exploration, the probabilities within Θ to sample the pragma values are initialized to Uniform at the beginning of the *DIDAHLs* process. New designs are synthesized to augment the dataset D in each iteration. To avoid excessive workloads from redundant design samples with `arrbound` containing the loop bounds, we constrain the design sampling process under three HLS rules [33], [39]:

- 1) If a loop is pipelined, all of its nested loops will be fully unrolled and not pipelined.
- 2) Pipelining and fully unrolling are mutually exclusive for the same loop.
- 3) Loops with variable bounds prevent pipelining the loops of the levels above.

B. DIDAHLs

We propose *DIDAHLs* for implementing the algorithm A illustrated in Eq. 6 to iteratively update Θ in order to sample designs d with minimal costs. The method overview is illustrated in Fig. 3.

```

void foo(float data_1[2][4][8], float data_2[2][4][8]){
  loop_0: for(int i=0; i<2; i++)
    loop_1: for(int j=0; j<4; j++)
      loop_2: for(int k=0; k<8; k++)
        data_2[i][j][k]=data_1[i][j][k];
}

```

Fig. 2. An example code with loop labels for HLS.

The pseudocode in Alg. 1 summarizes *DID4HLS*. A set of optimization weights λ sweeping from 0 to 1 is pre-defined in order to approximate Pareto front. The arrays introduced in the section IV-A are pre-defined to determine the design space S for each benchmark, and then a set of distributions Θ , each Θ_k corresponding to λ_k , are initialized to Uniform (line 3). n_1 pragma configurations are sampled from Θ under the constraint of the three sampling rules. The algorithm in C++ code combining each configuration gives a design d . All of them form a set $\{d\}_{n_1}$ (line 6). We invoke the HLS tool to synthesize the designs from $\{d\}_{n_1}$ that are new to D (lines 7-8). The synthesis results include PIR CDFG g , design latency l and area a , and the Θ vectors under which the configurations are sampled (line 11). They are collected into D (line 12). Then, l and a are standardized (line 13). Two predictors $P_l(g)$ and $P_a(g)$ are trained with D for predicting standardized l and a , respectively (line 14). The model training takes g as input, standardized l and a as ground truth. Each predictor comprises two parts: an extractor, $F_l(g)$ or $F_a(g)$, for extracting graph feature \mathbf{f}_l or \mathbf{f}_a , and an MLP, $MLP_l(\mathbf{f}_l)$ or $MLP_a(\mathbf{f}_a)$, for predicting l or a . After training the predictors, \mathbf{f}_l and \mathbf{f}_a of the synthesized designs are extracted (line 15), combined with corresponding Θ vectors, for training two estimators V_l and V_a that reconstruct \mathbf{f}_l and \mathbf{f}_a conditioned on Θ_k (line 16). Then, we build a surrogate based on MLP_l , MLP_a , and the decoders Dec_l of V_l and Dec_a of V_a . n_2 prior samples $\{\mathbf{z}_i\}$, combined with Θ_k of current iteration, result in \hat{c}_k as the estimation of the cost c_k (lines 18-21). Through gradient descent with respect to \hat{c}_k , Θ_k is updated for several times, where we build a function η with the aid of the ADAM optimizer [40] to output updating rates while guaranteeing validity of Θ_k (line 22). In the next iteration, if the synthesis budget B is reached, an approximate Pareto front will be returned (lines 9-10).

C. Predictors

Fig. 4 illustrates the predictor architecture. We construct $F_l(g)$ and $F_a(g)$, each with three layers of GATv2 which demonstrates state-of-the-art performance when applied to graph data [30]. An ELU activation layer is applied between two adjacent GATv2 layers [41]. Before the PIR data are input into the deep models, their node and edge attributes are embedded.

GATv2 updates the node features through the normalized attention weights:

$$\alpha_{i,j} = \frac{\exp[\mathbf{a}^\top \text{LeakyReLU}(\mathbf{W}[\mathbf{h}_i \parallel \mathbf{h}_j \parallel \mathbf{e}_{i,j}])]}{\sum_{k \in N(i) \cup \{i\}} \exp[\mathbf{a}^\top \text{LeakyReLU}(\mathbf{W}[\mathbf{h}_i \parallel \mathbf{h}_k \parallel \mathbf{e}_{i,k}])]} \quad (7)$$

where $\mathbf{e}_{i,j}$ denotes the edge attribute from node i to j , $N(i)$ denotes one-hop neighbor nodes of node i . The mean

Algorithm 1 *DID4HLS*

- 1: **Input:** C++ code with loop labels, arrays determining design space S , synthesis budget B , batch size n_1 and n_2 , optimization weights λ
- 2: **Output:** Approximate Pareto front
- 3: Initialize $\Theta_k \sim \text{Uniform}$
- 4: Dataset $D = \emptyset$
- 5: **repeat**
- 6: n_1 samples from Θ : $\{d\}_{n_1}$
- 7: $\{d\}_{new} = \{d\}_{n_1} \setminus (\{d\}_D \cap \{d\}_{n_1})$
- 8: Invoke HLS tool on $\{d\}_{new}$
- 9: **if** Number of synthesized designs == B :
- 10: **return** approximate Pareto front
- 11: $D_{new} = \{[g, l, a, \{\Theta_k\}]_{d\}_{new}$
- 12: $D \leftarrow D \cup D_{new}$
- 13: Standardize $l, a \in D$
- 14: Train P_l and P_a with $g, l, a \in D$
- 15: Extract $\mathbf{f}_l = F_l(g)$ and $\mathbf{f}_a = F_a(g)$ with $g \in D$
- 16: Train V_l and V_a with $\mathbf{f}_l, \mathbf{f}_a$, and $[\Theta_k]_d \in D$
- 17: **repeat**
- 18: n_2 samples from $p(\mathbf{z})$: $\{\mathbf{z}_i\}$, $i = 1, 2, \dots, n_2$
- 19: $\hat{l}_i = MLP_l(Dec_l(\mathbf{z}_i, \Theta_k))$
- 20: $\hat{a}_i = MLP_a(Dec_a(\mathbf{z}_i, \Theta_k))$
- 21: $\hat{c}_{ki} = \lambda_k \hat{l}_i + (1 - \lambda_k) \hat{a}_i$
- 22: $\Theta_k \leftarrow \Theta_k - \eta(\Theta_k) \sum_{n_2} \partial \hat{c}_{ki} / \partial \Theta_k$

aggregation of features from all nodes results in the graph feature \mathbf{f} . Then an MLP follows to predict the objectives. It is important to note that the predictors are trained for feature extraction and not for DSE, since their training data are obtained after HLS.

D. Estimators

Following the training of P_l and P_a , F_l and F_a extract graph features \mathbf{f} of $g \in D$. Then \mathbf{f} and Θ vectors under which the designs are sampled are adopted to train V_l and V_a based on VAE for learning conditional distributions of \mathbf{f} . The architecture of these estimators is illustrated in Fig. 5, wherein Dec realizes μ in Eq. 3, \mathbf{m} and \mathbf{v} realize m_i and v_i respectively in Eq. 3 across all dimensions i . We assume the prior distribution as $p(\mathbf{z}) = N(\mathbf{0}, \mathbf{I})$ [37]. After training, the combination of a prior sample $\mathbf{z} \sim p(\mathbf{z})$ and Θ_k transformed by an MLP projector as input into a decoder yields a sample of \mathbf{f} from the estimated distribution.

V. EXPERIMENTS

A. Benchmarks

Our method emphasizes optimization on algorithms characterized by compute-intensive traits. As such, we evaluated *DID4HLS* using six benchmarks adapted from PolyBench and MachSuite:

- 1) *correlation* has three sets of complex loop nests with intensive computation, introducing diversity in the loop structures. Its loop optimization requires bandwidth match from memory access arrangement.

Estimators are trained based on the trained predictors, after which all the trained models are adopted to update the distributions with gradient descent

The dataset containing the synthesized designs for training predictors and estimators

After HLS of the new designs, their PIR CDFGs, objectives, and corresponding distributions augment the dataset

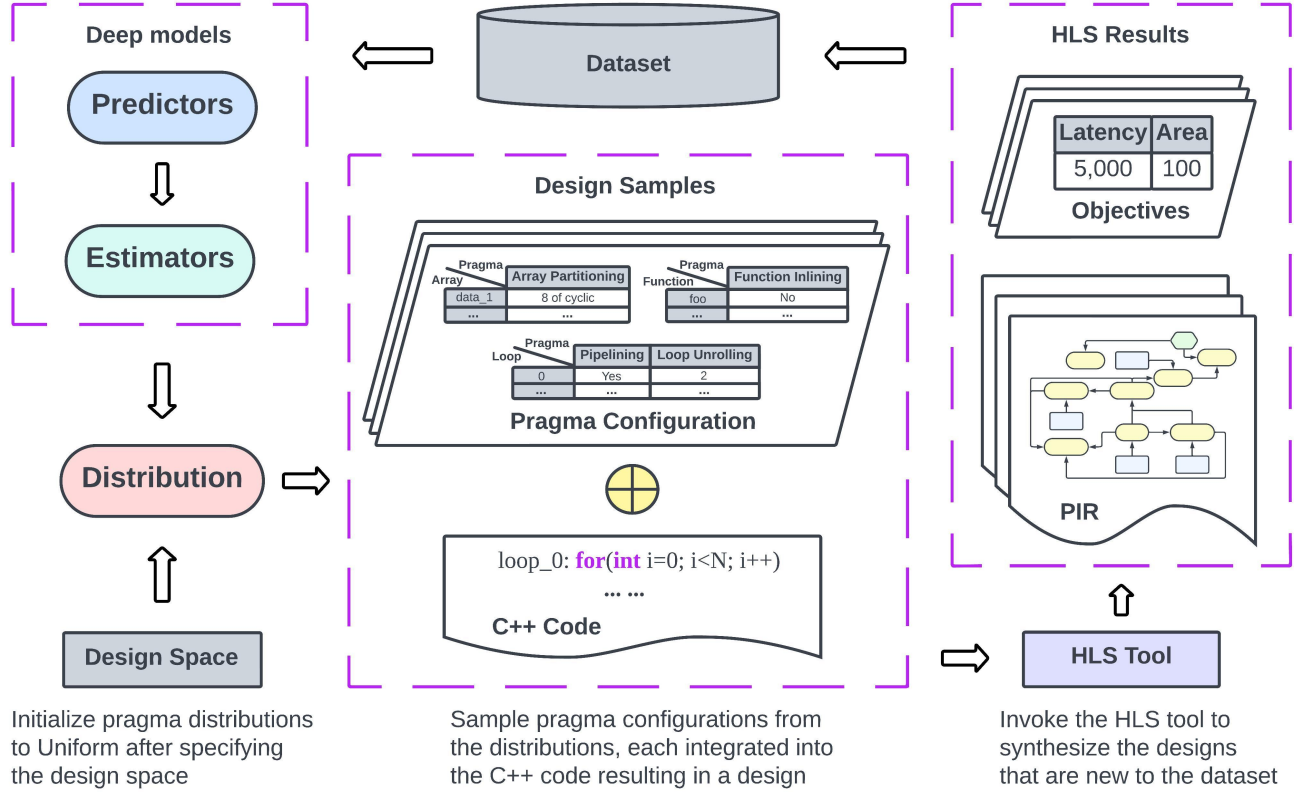


Fig. 3. Overview of DID4HLS. After specifying the design space of an algorithm, the corresponding distributions Θ for sampling pragma configurations are initialized to Uniform. In each iteration, the configurations are combined with the algorithm to generate designs described in C++. Invoking HLS tools generates the PIRs and objectives to augment the dataset for training the predictors and estimators, based on which a surrogate is constructed for updating Θ , concluding the current iteration.

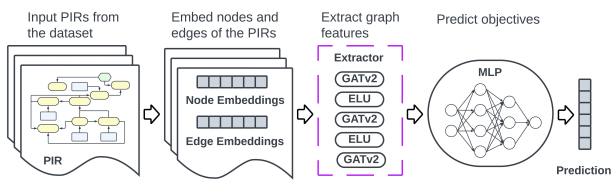


Fig. 4. Architecture of the predictors. The PIR CDFGs extracted from HLS results are embedded before input into the deep model based on GATv2. The model then outputs graph features for the following MLP to predict the objectives.

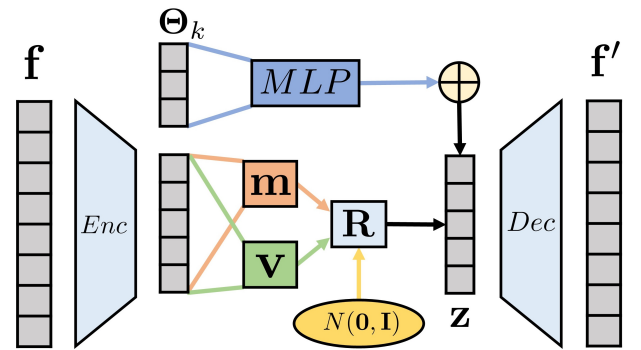


Fig. 5. Architecture of the estimators based on VAE. \mathbf{m} and \mathbf{v} output the mean and variance respectively of the Gaussian approximation. The node \mathbf{R} signifies the reparameterization trick. Enc represents the encoder. Dec represents the decoder tasked with reconstruction of the graph features \mathbf{f} , denoted as \mathbf{f}' .

2) *covariance* has two sets of complex loop nests with intensive computation. Its complex data access pattern enlarges room of optimization on parallelization.

3) *gramSchmidt* has one loop nest with five levels performing complicated calculations. The challenges related to both the depth and intricacy of the loop structure include addressing data dependencies and managing loop overhead.

4) *aes* is implemented by a flattened loop structure containing nine loops, six of which are wrapped inside functions. This structure increases opportunities for scheduling and resource sharing due to direct data dependencies and frequent function

calls.

5) *sort_radix* heavily depends on memory access patterns. Optimization on loops, arrays, and function calls improves the efficiency in rearranging the data based on digit positions.

6) *stencil_3d* operates three-dimensional datasets, introducing

complex data access patterns. Loop and array optimizations enhance its spatial locality.

The benchmarks and their design spaces tested in our work are accessible on [gitHub](https://github.com)¹.

B. Metric for evaluation

We adopt ADRS for evaluating the methods in our work [3], [4]. A design is said to be non-dominated if there is no other design that improves one objective, e.g., latency and area, without worsening the other, and Pareto front is the set of all such non-dominated designs. ADRS calculates the distance from an approximate Pareto front to the reference Pareto front:

$$ADRS(\Gamma, \Omega) = (1/|\Gamma|) \sum_{\gamma \in \Gamma} \min_{\omega \in \Omega} f(\gamma, \omega) \quad (8)$$

where $f(\gamma, \omega) = \max\{|\frac{a_\omega - a_\gamma}{a_\gamma}|, |\frac{l_\omega - l_\gamma}{l_\gamma}|\}$, Γ is the reference Pareto front, and Ω is the approximate Pareto front. For each benchmark, Ω is obtained from the synthesis results of all the tests conducted by one method or ablation configuration, and we obtain Γ from all the Ω datasets. We do not exhaustively search the design spaces because they are too large. For example, that of *stencil_3d* contains over 10^{15} designs. Smaller ADRS denotes closer distance and better performance.

C. Comparison with the baselines

The two predictors in *DID4HLS* share identical architecture, one for latency (measured in clock cycles) and the other for area (measured in the count of FF, LUT, DSP, BRAM and URAM). The GATv2 layers are implemented using the PyG library [42].

In our method, we set $\lambda = [0, 0.2, 0.4, 0.6, 0.8, 1]$ to approximate the Pareto front. In each iteration, 5 designs are sampled for each optimization weight and 30 designs in total are synthesized. The PIR CDFGs are extracted from the **.adb* files. We choose four state-of-the-art DSE methods for HLS as the baselines for the comparative analysis. All the baselines share the same design sampling process as *DID4HLS* for a fair comparison. We introduce the baselines and provide their implementations below:

1) *GRASP* [43] is a tree-based heuristic method composed of two steps: Greedy Randomized Construction (GRC) and Local Search (LS). In each iteration, GRC creates a Restricted Candidate List (RCL) containing the most promising pragmas with minimum costs that are estimated by the predictor based on a decision tree. Then the LS phase further refines the pragmas based on the RCL. All the newly synthesized designs update the predictor for the next iteration. We set 100 estimators for the random forest regressor, cost distance α as 0.7, and RCL synthesis interval as 8. At the beginning, we randomly sample 120 designs and synthesize them to train the predictor. Then we start the GRASP process in iterations until the synthesis budget is reached.

2) *AutoHLS* [44] constructs predictors with MLP for performance and synthesizability scores of designs. Based on the performance predictor, Bayesian optimization is applied

to pragmas and approximates a Pareto front, implemented by Optuna [45]. In the first iteration, we randomly sample and synthesize 30 designs to train the predictors. We operate synthesizability scores as the probabilities of designs to be successfully synthesized, and set the threshold as 0.5. We synthesize 30 designs from the approximate Pareto front whose scores are predicted over the threshold. After synthesis, we update the models and start the next iteration.

3) *SA-ML* [16] is an annealing-based method. The predictive models are based on XGBoost [46]. We adopt Clang² to compile the C++ code with pragmas into LLVM IRs. Then, the design features as the model input are extracted from the IR CDFGs through Programl [20], including attributes such as node counts of each type, path length, and pipelining weight. We set the initial temperature to 10 with a temperature change rate of 0.1 and 50 runs at each temperature. The predictive models are trained with an initial set of 150 designs randomly sampled and synthesized. Hyperparameter tuning is conducted using Comet.ml with Bayesian optimization³. We define a set of 30 optimization weights evenly spaced between 0 and 1 to approximate a Pareto front, and randomly sample 30 designs as the starting point for each weight. Through simulated annealing, each design transitions to its neighbor by randomly selecting one of its pragma and changing to an adjacent value until the stopping condition, which is set to 500 rejects or the temperature of 10^{-7} . The candidates are synthesized after the final transitions.

4) *GNN-DSE* [13] is an exhaustive search method with a GNN surrogate. We adopt Clang to compile C++ code with pragmas into LLVM IRs. Their CDFGs, obtained through Programl, are input into the GAT-based models for predictions. The feature selection mechanism Jumping Knowledge Network (JKN) identifies dominant node features from the GAT layers [35] and maps them into graph features. Subsequently, an MLP follows to output predictions. We construct two separate models to predict latency and area. The models are trained with an initial set of 150 designs randomly sampled and synthesized. In the DSE phase, we randomly sample 5,000 designs and predict their latency and area with the trained models. Then, we approximate a Pareto front and randomly select 30 designs from the front to synthesize.

Tab. I summarizes the performance comparison between *DID4HLS* and the baselines. Our method performed the best on all the benchmarks. The average ADRS improvement achieved by *DID4HLS* is 42.5%, with up to 53.9% for *aes*. In the worst case (*stencil_3d*), our method improved the ADRS by 31.1%. To further demonstrate the effectiveness of our work, Fig. 6 shows the distances of the approximate Pareto fronts by *DID4HLS* and the best-performing baselines to the reference Pareto front. Our method obtained the optimal balance between latency and area for *correlation*, and these designs overlap the reference Pareto points. Our method achieved more Pareto points than the best-performing baseline for *covariance* (16 vs. 6), leaving more room for design trade-offs. For *aes*, our method outperforms the best-performing

¹<https://github.com/PingChang818/DID4HLS>

²<https://clang.llvm.org>

³<https://www.comet.com>

baseline to such an extent that a gap forms between their respective fronts. Therefore, *DID4HLS* demonstrates the superior performance and robustness in improving design QoR.

We also compared the time consumed by each method. Fig. 7 lists the average time over all the benchmarks. We set the synthesis timer to five minutes, indicating that the design synthesis process will be terminated if it is not completed within this timeframe. *AutoHLS* consumed the least time of 30.5 minutes. *SA-ML* consumed the most time with 145.5 minutes. Our method consumed 48.0 minutes, achieving high efficiency.

D. Ablation study

Generative models are particularly relevant for learning conditional distributions, among which VAE, Generative Adversarial Network (GAN), and diffusion model have demonstrated state-of-the-art performance [37], [47], [48]. Therefore, we conducted an ablation study to compare their performance.

GAN consists of a generator and a discriminator. The generator takes random noise as input and generates samples similar to the training data. The discriminator is responsible for distinguishing the generated samples from the real. As training proceeds, both the generator and discriminator improve at their respective tasks. Fig. 8 shows the structure of GAN-based estimators, wherein both the generator and discriminator have their own MLP projector that transforms Θ_k into a vector concatenated to the input for learning the conditional distribution, f' denotes the generated graph feature whose ground truth f is obtained from the extractor of the predictor. After training, we adopt the generator to build the surrogate.

Diffusion model stems from the idea that a continuous Gaussian diffusion process can be reversed with the same functional form as the forward process. The reverse process converges pure noise to samples in the target distribution. The diffusion process can be approximated with a discrete process given enough diffusion steps. The backbone of diffusion model is responsible for extracting meaningful features from the input data at various diffusion steps to iteratively remove noise. Fig. 9 shows the backbone structure we adapted from *DiffWave* [49], because the gated structure excels at filtering out critical information from the input data, meanwhile skip connections mitigate the vanishing and exploding gradient problems and capture information at multiple levels of abstraction [49]–[51]. We set the number of diffusion steps as 50 with a quadratic noise schedule from $\beta_1 = 10^{-4}$ to $\beta_{50} = 0.5$ [50], [51].

To demonstrate the benefits of PIR over LLVM IR in our work, we also conducted a comparative experiment to explore PIR’s representational power. In this experiment, we compile the sampled designs into LLVM IR, instead of PIR, to train the predictors, while the estimators are based on VAE.

Tab. II lists the ADRS values of the ablation configurations, showing the performance to approximate the Pareto fronts achieved by using GAN vs. VAE, diffusion model vs. VAE, and LLVM IR vs. PIR. The complexities of the GAN-based and diffusion model-based estimators are aligned with that

of the VAE-based estimators using PyTorch-OpCounter⁴, each having around three million parameters. The results show the superior performance of PIR combined with VAE. The average improvement is 48.0% over the best-performing ablation configurations, with up to 58.2% improvement for *gramSchmidt*. The least improvement is 35.6% for *stencil_3d*.

For each benchmark, we set the synthesis budget to be 180 solutions for all the methods and ablation configurations. We made modifications to the open-sourced code of *GRASP*⁵, and re-implemented the remaining baselines as closely as possible according to their respective descriptions. All the experiments were implemented using Python on the PyTorch framework [41]. The computational hardware utilized included an Intel i7-12700K processor for HLS and an Nvidia RTX 3090 graphics card for training deep models. We used Vitis HLS as the HLS tool. Our simulation platform was set as the Defense-grade Virtex-7Q FPGA with part number xq7vx690t-rf1930-1I, with a clock constraint of $10n.s$. All built-in automatic optimizations were disabled.

VI. DISCUSSION

The input data for the predictive models in *GRASP* are only pragma configurations. It is hard to iterate toward optimal direction with a limited synthesis budget. Then, designs from LS are easily stuck at local optimum. The surrogate models of *AutoHLS* are hard to capture the complex interactions between pragmas and designs, leading to the inferior performance by the Bayesian optimization. However, the simple input format for the deep models in *AutoHLS*, combined with the high efficiency of Bayesian optimization, results in superior speed performance. *SA-ML* combines simulated annealing and the predictive models for code analysis in LLVM IR, but fails to leverage information from the HLS processes. The sequential nature of its annealing process largely impacts the speed and *SA-ML* consumes the most time. The original implementation of *GNN-DSE* depends on predictive models pre-trained with large datasets. However, in our work, we constrained the training dataset to a small size and observed the overall performance behind *DID4HLS*. This highlights the effectiveness of *DID4HLS* in capturing HLS behaviors. Our method not only achieves the best QoR, but also operates within a reasonable time frame, demonstrating an optimal trade-off between performance and speed.

GAN, while effective, is known to face challenges such as discriminator overfitting and training stability issues, especially in the cases of limited data availability [52], [53]. Due to the time-consuming nature of HLS, there is usually a scarcity of training data. The dataset is updated in each iteration and the model must be re-trained thereafter. Thus, the stability issues may accumulate throughout the optimization process and lead to failure in finding the directions along which the distributions converge toward the Pareto front. While diffusion model generates samples with high fidelity and diversity, the stochasticity introduced by multiple diffusion

⁴<https://github.com/Lyken17/pytorch-OpCounter>

⁵https://github.com/nibst/GRASP_DSE

TABLE I

ADRS OF ALL METHODS IN THE COMPARATIVE EXPERIMENTS. BOLD FONT HIGHLIGHTS THE LOWEST (BEST) VALUES. OUR METHOD PERFORMED THE BEST AND ITS IMPROVEMENT OVER THE BEST-PERFORMING BASELINES ARE LISTED.

Method	<i>correlation</i>	<i>covariance</i>	<i>gramSchmidt</i>	<i>aes</i>	<i>sort_radix</i>	<i>stencil_3d</i>
<i>GRASP</i>	0.404	0.599	0.282	0.387	0.676	0.492
<i>AutoHLS</i>	0.378	0.546	0.387	0.232	0.964	0.506
<i>SA-ML</i>	0.639	1.148	0.199	0.335	0.307	0.498
<i>GNN-DSE</i>	0.551	0.365	0.266	0.491	0.374	0.426
<i>DID4HLS (ours)</i>	0.199	0.209	0.115	0.107	0.191	0.325
Improvement	47.4%	42.7%	42.2%	53.9%	37.8%	31.1%

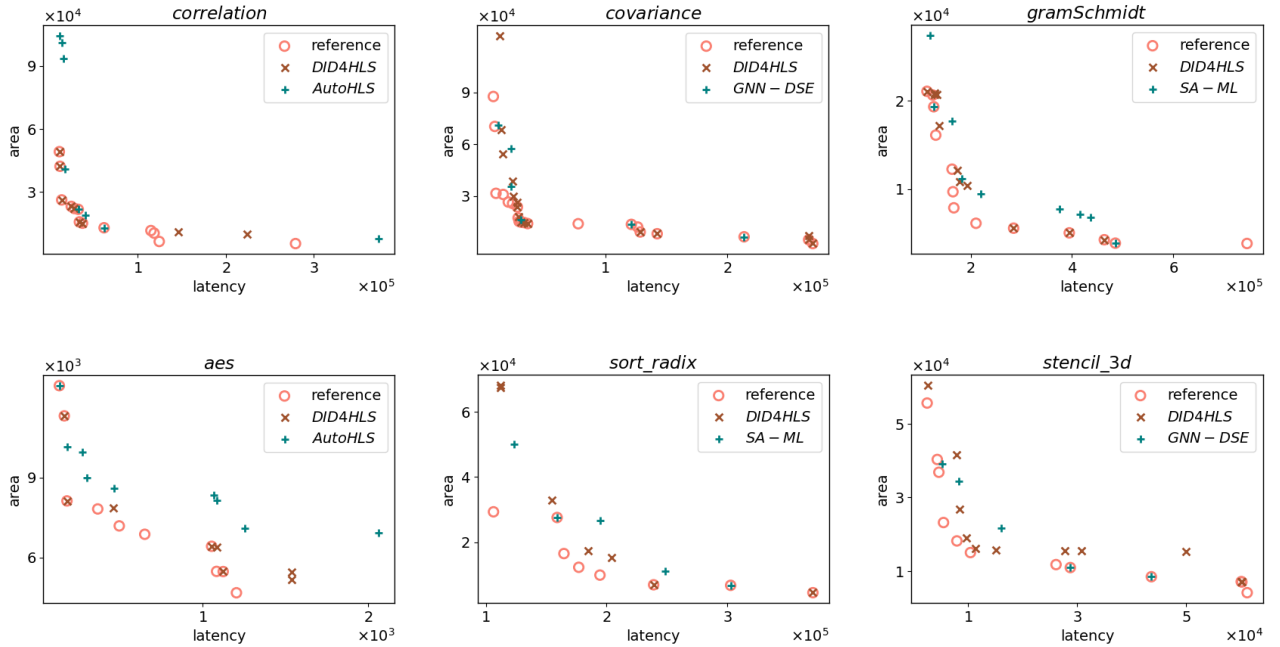


Fig. 6. Comparison between our method and the baselines shows the superior performance of our method, where \circ denotes reference Pareto front, \times and $+$ denote approximate Pareto front of our method and the best-performing baseline respectively.

TABLE II

ADRS OF ALL CONFIGURATIONS FOR THE ABLATION STUDY. BOLD FONT HIGHLIGHTS THE LOWEST (BEST) VALUE. PIR + VAE PERFORMS THE BEST AND WE ADOPT IT IN OUR METHOD.

Method	<i>correlation</i>	<i>covariance</i>	<i>gramSchmidt</i>	<i>aes</i>	<i>sort_radix</i>	<i>stencil_3d</i>
PIR + GAN	0.706	1.156	0.484	0.289	0.472	0.672
PIR + diffusion model	0.729	0.727	0.275	0.431	0.484	0.890
LLVM IR + VAE	0.468	0.327	0.310	0.201	0.413	0.505
PIR + VAE (ours)	0.199	0.209	0.115	0.107	0.191	0.325
Improvement	57.5%	36.1%	58.2%	46.8%	53.8%	35.6%

AutoHLS	30.5
GRASP	62.1
SA – ML	145.5
GNN – DSE	39.5
DID4HLS (ours)	48.0

Fig. 7. The average time in minutes over all the benchmarks consumed by each method.

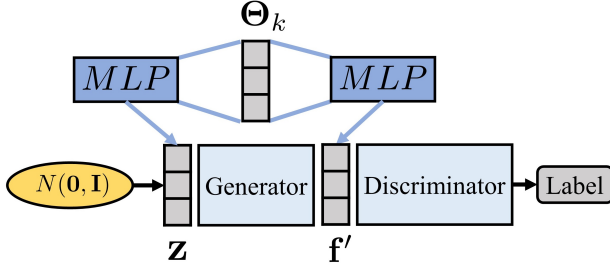


Fig. 8. Architecture of the estimators based on GAN. The generator and discriminator are constructed with MLP

steps hinders the reparameterization trick during the gradient-based update of the distributions. LLVM IR combined with VAE performs far behind *DID4HLS*, indicating the limitation of feature extraction from LLVM IR and the importance of using PIR to leverage post-HLS information.

There is still room for improving *DID4HLS*. Although it does not depend on a specific compiler to generate IR graphs, transitioning to platforms other than Vitis HLS will necessitate the development of new interfaces parsing the HLS solutions. This issue may hinder the portability of our method. The other issue is that when optimizing larger designs, their PIR CDFGs will be exponentially more complicated. This may be a great burden for our predictors, requiring more computational resources or slowing the optimization. These issues highlight the importance of considering technical limitations in trade-offs between effectiveness and speed when selecting DSE methods for HLS.

To further improve our method, we may also expand the design space accommodating more pragmas such as array reshaping, loop tiling, and data flow. We may also port *DID4HLS* to other platforms for additional validation. Implementation of hyperparameter tuning, transfer learning, and online training

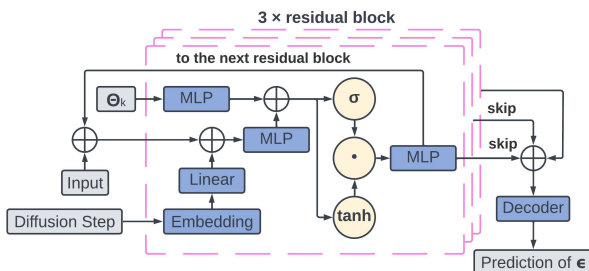


Fig. 9. Backbone structure of the diffusion model-based estimators. The Gaussian noise $\epsilon \sim N(0, I)$.

may be considered to explore more potential.

VII. CONCLUSION

In this work, we propose *DID4HLS*, a method that learns HLS behaviors, enabling design samples to iterate toward the Pareto front with a low synthesis budget. We demonstrate the effectiveness of *DID4HLS* with its improvement on design QoR through the tuning of pragmas for loop pipelining, loop unrolling, array partitioning, and function inlining. The comparative experiments exhibit the superior performance of our method over the four state-of-the-art baselines. It achieved an average improvement of 42.5% on ADRS over the best-performing baselines with high robustness and efficiency. In addition, the ablation study validated the construction of *DID4HLS*.

REFERENCES

- [1] Sharad Sinha and Thambipillai Srikanthan. High-level synthesis: Boosting designer productivity and reducing time to market. *IEEE Potentials*, 34(4):31–35, 2015. I
- [2] Sakari Lahti, Panu Sjövall, Jarno Vanne, and Timo D Hämäläinen. Are we there yet? a study on the state of high-level synthesis. *IEEE Transactions on Computer-Aided Design of Integrated Circuits and Systems*, 38(5):898–911, 2018. I
- [3] Benjamin Carrion Schafer and Zi Wang. High-level synthesis design space exploration: Past, present, and future. *IEEE Transactions on Computer-Aided Design of Integrated Circuits and Systems*, 39(10):2628–2639, 2019. I, V-B
- [4] Yuchao Liao, Tosiron Adegbiya, and Roman Lysecky. Efficient system-level design space exploration for high-level synthesis using pareto-optimal subspace pruning. In *Proceedings of the 28th Asia and South Pacific Design Automation Conference*, pages 567–572, 2023. I, V-B
- [5] Anushree Mahapatra and Benjamin Carrion Schafer. Machine-learning based simulated annealer method for high level synthesis design space exploration. In *Proceedings of the 2014 Electronic System Level Synthesis Conference (ESLsyn)*, pages 1–6. IEEE, 2014. I
- [6] Sotirios Xydis, Christos Skouroumounis, Kiamal Pekmestzi, Dimitrios Soudris, and George Economakos. Efficient high level synthesis exploration methodology combining exhaustive and gradient-based pruned searching. In *2010 IEEE Computer Society Annual Symposium on VLSI*, pages 104–109. IEEE, 2010. I
- [7] Benjamin Carrion Schafer. Probabilistic multiknob high-level synthesis design space exploration acceleration. *IEEE Transactions on Computer-Aided Design of Integrated Circuits and Systems*, 35(3):394–406, 2015. I
- [8] Nam Khanh Pham, Amit Kumar Singh, Akash Kumar, and Mi Mi Aung Khin. Exploiting loop-array dependencies to accelerate the design space exploration with high level synthesis. In *2015 Design, Automation & Test in Europe Conference & Exhibition (DATE)*, pages 157–162. IEEE, 2015. I
- [9] Lorenzo Ferretti, Giovanni Ansaloni, and Laura Pozzi. Cluster-based heuristic for high level synthesis design space exploration. *IEEE Transactions on Emerging Topics in Computing*, 9(1):35–43, 2018. I
- [10] Cody Hao Yu, Peng Wei, Max Grossman, Peng Zhang, Vivek Sarker, and Jason Cong. S2fa: An accelerator automation framework for heterogeneous computing in datacenters. In *Proceedings of the 55th Annual Design Automation Conference*, pages 1–6, 2018. I
- [11] Srikanth Kurra, Neeraj Kumar Singh, and Preeti Ranjan Panda. The impact of loop unrolling on controller delay in high level synthesis. In *2007 Design, Automation & Test in Europe Conference & Exhibition*, pages 1–6. IEEE, 2007. I
- [12] Zonghan Wu, Shirui Pan, Fengwen Chen, Guodong Long, Chengqi Zhang, and S Yu Philip. A comprehensive survey on graph neural networks. *IEEE transactions on neural networks and learning systems*, 32(1):4–24, 2020. I
- [13] Atefeh Sohrabzadeh, Yunsheng Bai, Yizhou Sun, and Jason Cong. Robust gnn-based representation learning for hls. In *2023 IEEE/ACM International Conference on Computer Aided Design (ICCAD)*, pages 1–9. IEEE, 2023. I, II-B, V-C

- [14] Ricardo Nobre, Luiz GA Martins, and João MP Cardoso. A graph-based iterative compiler pass selection and phase ordering approach. *ACM SIGPLAN Notices*, 51(5):21–30, 2016. I
- [15] Lorenzo Ferretti, Andrea Cini, Georgios Zacharopoulos, Cesare Alippi, and Laura Pozzi. Graph neural networks for high-level synthesis design space exploration. *ACM Transactions on Design Automation of Electronic Systems*, 28(2):1–20, 2022. I
- [16] Pingakshya Goswami, Benjamin Carrion Schaefer, and Dinesh Bhatia. Machine learning based fast and accurate high level synthesis design space exploration: From graph to synthesis. *Integration*, 88:116–124, 2023. I, V-C
- [17] Chris Lattner and Vikram Adve. Llvm: A compilation framework for lifelong program analysis & transformation. In *International symposium on code generation and optimization, 2004. CGO 2004.*, pages 75–86. IEEE, 2004. I
- [18] Fanny Chevalier, David Auber, and Alexandru Telea. Structural analysis and visualization of c++ code evolution using syntax trees. In *Ninth international workshop on Principles of software evolution: in conjunction with the 6th ESEC/FSE joint meeting*, pages 90–97, 2007. I
- [19] Ron Cytron, Jeanne Ferrante, Barry K Rosen, Mark N Wegman, and F Kenneth Zadeck. An efficient method of computing static single assignment form. In *Proceedings of the 16th ACM SIGPLAN-SIGACT symposium on Principles of programming languages*, pages 25–35, 1989. I
- [20] Chris Cummins, Zacharias V Fisches, Tal Ben-Nun, Torsten Hoefler, Michael FP O’Boyle, and Hugh Leather. Programl: A graph-based program representation for data flow analysis and compiler optimizations. In *International Conference on Machine Learning*, pages 2244–2253. PMLR, 2021. I, V-C
- [21] Yun Liang, Shuo Wang, and Wei Zhang. Flexcl: A model of performance and power for opencl workloads on fpgas. *IEEE Transactions on Computers*, 67(12):1750–1764, 2018. I
- [22] Michael C McFarland, Alice C Parker, and Raul Camposano. Tutorial on high-level synthesis. In *Proceedings of the 25th ACM/IEEE Design Automation Conference*, pages 330–336, 1988. I
- [23] Ruifan Xu, Youwei Xiao, Jin Luo, and Yun Liang. Hector: A multi-level intermediate representation for hardware synthesis methodologies. In *Proceedings of the 41st IEEE/ACM International Conference on Computer-Aided Design*, pages 1–9, 2022. I
- [24] Erez Gershonabel, Mingkun Chen, Chenkai Mao, Evan W Wang, Philippe Lalanne, and Jonathan A Fan. Reparameterization approach to gradient-based inverse design of three-dimensional nanophotonic devices. *ACS Photonics*, 10(4):815–823, 2022. I
- [25] Sean Molesky, Zin Lin, Alexander Y Piggott, Weiliang Jin, Jelena Vucković, and Alejandro W Rodriguez. Inverse design in nanophotonics. *Nature Photonics*, 12(11):659–670, 2018. I
- [26] Haoyu Peter Wang, Nan Wu, Hang Yang, Cong Hao, and Pan Li. Unsupervised learning for combinatorial optimization with principled objective relaxation. *Advances in Neural Information Processing Systems*, 35:31444–31458, 2022. I
- [27] Chris J Maddison, Andriy Mnih, and Yee Whye Teh. The concrete distribution: A continuous relaxation of discrete random variables. *arXiv preprint arXiv:1611.00712*, 2016. I
- [28] Zhe Lin, Jieru Zhao, Sharad Sinha, and Wei Zhang. Hl-pow: A learning-based power modeling framework for high-level synthesis. In *2020 25th Asia and South Pacific Design Automation Conference (ASP-DAC)*, pages 574–580. IEEE, 2020. I, II-A
- [29] Huizhen Kuang, Xianfeng Cao, Jingyuan Li, and Lingli Wang. Hgbdse: Hierarchical gnn and bayesian optimization based hls design space exploration. In *2023 International Conference on Field Programmable Technology (ICFPT)*, pages 106–114. IEEE, 2023. I, II-A
- [30] Shaked Brody, Uri Alon, and Eran Yahav. How attentive are graph attention networks? *arXiv preprint arXiv:2105.14491*, 2021. I, II-B, II-B, IV-C
- [31] Miguel Á Abella-González, Pedro Carollo-Fernández, Louis-Noël Pouchet, Fabrice Rastello, and Gabriel Rodríguez. Polybench/python: benchmarking python environments with polyhedral optimizations. In *Proceedings of the 30th ACM SIGPLAN International Conference on Compiler Construction*, pages 59–70, 2021. I
- [32] Brandon Reagen, Robert Adolf, Yakun Sophia Shao, Gu-Yeon Wei, and David Brooks. Machsuite: Benchmarks for accelerator design and customized architectures. In *2014 IEEE International Symposium on Workload Characterization (IISWC)*, pages 110–119. IEEE, 2014. I
- [33] Vinod Kathail. Xilinx vitis unified software platform. In *Proceedings of the 2020 ACM/SIGDA International Symposium on Field-Programmable Gate Arrays*, pages 173–174, 2020. II-A, IV-A
- [34] Ashish Vaswani, Noam Shazeer, Niki Parmar, Jakob Uszkoreit, Llion Jones, Aidan N Gomez, Łukasz Kaiser, and Illia Polosukhin. Attention is all you need. *Advances in neural information processing systems*, 30, 2017. II-B
- [35] Petar Veličković, Guillem Cucurull, Arantxa Casanova, Adriana Romero, Pietro Lio, and Yoshua Bengio. Graph attention networks. *arXiv preprint arXiv:1710.10903*, 2017. II-B, V-C
- [36] Kurt Hornik. Approximation capabilities of multilayer feedforward networks. *Neural networks*, 4(2):251–257, 1991. II-B
- [37] Carl Doersch. Tutorial on variational autoencoders. *arXiv preprint arXiv:1606.05908*, 2016. II-C, IV-D, V-D
- [38] David M Blei, Alp Kucukelbir, and Jon D McAuliffe. Variational inference: A review for statisticians. *Journal of the American Statistical Association*, 112(518):859–877, 2017. II-C
- [39] AMD Xilinx. Vitis high-level synthesis user guide (ug1399), 2023. IV-A
- [40] Diederik P Kingma and Jimmy Ba. Adam: A method for stochastic optimization. *arXiv preprint arXiv:1412.6980*, 2014. IV-B
- [41] Adam Paszke, Sam Gross, Francisco Massa, Adam Lerer, James Bradbury, Gregory Chanan, Trevor Killeen, Zeming Lin, Natalia Gimelshein, Luca Antiga, et al. Pytorch: An imperative style, high-performance deep learning library. *Advances in neural information processing systems*, 32, 2019. IV-C, V-D
- [42] Matthias Fey and Jan Eric Lenssen. Fast graph representation learning with pytorch geometric. *arXiv preprint arXiv:1903.02428*, 2019. V-C
- [43] Níkolás P Schuster and Gabriel L Nazar. Grasp-based high-level synthesis design space exploration for fpgas. In *2023 XIII Brazilian Symposium on Computing Systems Engineering (SBESC)*, pages 1–6. IEEE, 2023. V-C
- [44] Md Rubel Ahmed, Toshiaki Koike-Akino, Kieran Parsons, and Ye Wang. Autohls: Learning to accelerate design space exploration for hls designs. *arXiv e-prints*, pages arXiv–2403, 2024. V-C
- [45] Takuya Akiba, Shotaro Sano, Toshihiko Yanase, Takeru Ohta, and Masanori Koyama. Optuna: A next-generation hyperparameter optimization framework. In *Proceedings of the 25th ACM SIGKDD international conference on knowledge discovery & data mining*, pages 2623–2631, 2019. V-C
- [46] Tianqi Chen and Carlos Guestrin. Xgboost: A scalable tree boosting system. In *Proceedings of the 22nd acm sigkdd international conference on knowledge discovery and data mining*, pages 785–794, 2016. V-C
- [47] Ian Goodfellow, Jean Pouget-Abadie, Mehdi Mirza, Bing Xu, David Warde-Farley, Sherjil Ozair, Aaron Courville, and Yoshua Bengio. Generative adversarial networks. *Communications of the ACM*, 63(11):139–144, 2020. V-D
- [48] Ling Yang, Zhilong Zhang, Yang Song, Shenda Hong, Runsheng Xu, Yue Zhao, Wentao Zhang, Bin Cui, and Ming-Hsuan Yang. Diffusion models: A comprehensive survey of methods and applications. *ACM Computing Surveys*, 2022. V-D
- [49] Zhifeng Kong, Wei Ping, Jiaji Huang, Kexin Zhao, and Bryan Catanzaro. Diffwave: A versatile diffusion model for audio synthesis. *arXiv preprint arXiv:2009.09761*, 2020. V-D, V-D
- [50] Yusuke Tashiro, Jiaming Song, Yang Song, and Stefano Ermon. Csd: Conditional score-based diffusion models for probabilistic time series imputation. *Advances in Neural Information Processing Systems*, 34:24804–24816, 2021. V-D, V-D
- [51] Ping Chang, Huayu Li, Stuart F Quan, Shuyang Lu, Shu-Fen Wung, Janet Roveda, and Ao Li. A transformer-based diffusion probabilistic model for heart rate and blood pressure forecasting in intensive care unit. *Computer Methods and Programs in Biomedicine*, page 108060, 2024. V-D, V-D
- [52] Tero Karras, Miika Aittala, Janne Hellsten, Samuli Laine, Jaakko Lehtinen, and Timo Aila. Training generative adversarial networks with limited data. *Advances in neural information processing systems*, 33:12104–12114, 2020. VI
- [53] Martin Arjovsky and Léon Bottou. Towards principled methods for training generative adversarial networks. *arXiv preprint arXiv:1701.04862*, 2017. VI